

# THERMAL/STRUCTURAL ANALYSIS OF A SRF PHOTOCATHODE ELECTRON GUN CAVITY<sup>1</sup>

T. Schultheiss, M. Cole, J. Rathke,  
Advanced Energy Systems, Medford, NY11763, USA

## Abstract

The novel Superconducting Photocathode Electron Gun being developed by Advanced Energy Systems and Brookhaven National Laboratory was analyzed to determine surface temperature and stress levels from RF and laser heat loads while being cooled in a helium bath. Optimization of geometry with respect to thermal loads was required when looking at 4.2K vs. 1.8K bath temperature. Heat loads were developed from a SUPERFISH model and were determined for surface temperatures between 2K and 8K. These heat loads were included in the model as a function of the RF surface temperature requiring a non-linear solution. Material properties such as thermal conductivity were also included as a function of temperature. The laser load on the cathode surface dominates the loads from RF and therefore, a constant load is used in this region. Results show that the temperature of the cathode will not adversely affect the superconductivity of the cavity. Uncertainty of the coolant effectiveness requires that the laser power be increased at a slow rate. The geometry of the back of the cathode where it is in contact with the helium bath is critical and will be evaluated during the testing phase of the program.

## 1 INTRODUCTION

Linear accelerators using superconducting radio frequency (SRF) cavities are the preferred method when high average beam currents are to be accelerated to high energies and when high-brightness beams are required. SRF linacs can transport the highest average currents, minimize emittance growth, minimize beam spill because of the large inter-cavity apertures that can be used, lead to better phase and amplitude stability because of the high stored energy of the cavities and can support the highest “real-estate” accelerating gradients; thereby leading to the brightest, most efficient and most compact accelerator system for the given application.

In this project we are evaluating integration of the photocathode into the SRF cavity. This will provide a substantial improvement in performance and efficiency as compared to using a normal conducting RF gun or other electron source to inject into a superconducting RF accelerator. Operating costs will be substantially less

than for a normal conducting RF gun because of the much lower losses in the SRF gun and the elimination of the need for high-power CW RF sources. The concept avoids mixed technology (superconducting and normal conducting RF) resulting in a simpler design, so that the entire injector will be considerably more compact than existing injectors. Since no foreign material is introduced into the superconducting environment and a complicated mounting structure is not required, the specific means of integration proposed here is an elegant solution as compared to other SRF photocathode gun schemes.

The focus of this paper is thermal and structural analysis used to determine the feasibility of this approach.

## 2 MODELING

The superconducting electron gun was analyzed thermally and structurally to determine surface temperature and stress levels from RF and laser heat loads while being cooled in a helium bath at 4.2K. Results from SUPERFISH in the form of heat loads as a function of temperature were applied to the cavity surfaces along with the laser power on the cathode.

A finite element thermal/structural model was developed using the same node and element connectivity for both the thermal and structural analysis. Figure 1 shows the structure that was analyzed, it includes the niobium cavity, stainless steel connection to the cryostat, Conflat flanges, and niobium stiffeners which were added

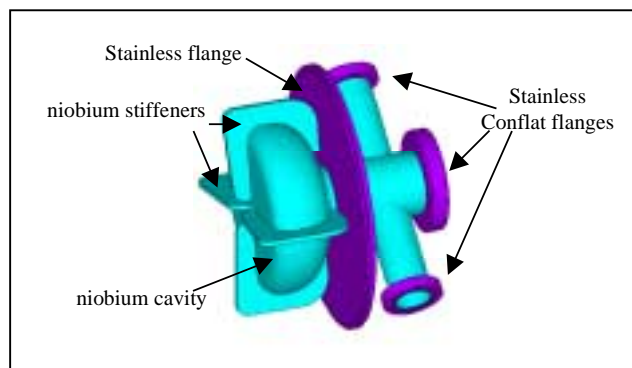


Figure 1, Electron Gun Model

to minimize deflection due to pressure differential.

Material properties of niobium and stainless are input as a function of temperature. Heat loads at temperatures

<sup>1</sup> The work discussed in this paper has been supported by the DOE SBIR Program, grant DE-FG02-99ER82724. Such support does not constitute an endorsement by DOE of the views expressed in this paper.

of 2K, 4.2K, 6K and 8K were developed from a SUPERFISH model. These heat loads were included in the model as a function of the RF surface temperature requiring a non-linear solution. The laser load on the cathode surface dominates the loads from RF and therefore, a constant laser load is applied. Heat flux surface segments are shown in figures 2 and 3 and their corresponding loads are given in Table 1.

Table 1, Segment Heat Loads

Segment	Surface Heat Loads mW/cm <sup>2</sup>			
	2K	4.2K	6K	8K
2	.16	4.08	9.42	14.21
3	2.25	55.99	129.33	195.20
4	6.67	166.25	384.05	579.64
5	6.06	150.95	348.72	526.31
6	6.88	171.29	395.71	597.23
7	7.04	175.32	405.02	611.28
8	6.38	159.01	367.34	554.41
9	5.88	146.46	338.34	510.65
10	4.45	110.88	256.14	386.58
11	2.15	53.67	123.98	187.12
12	.02	.41	.94	1.42
13*	7560.	7560.	7560.	7560.
14*	5940.	5940.	5940.	5940.
15*	2440.	2440.	2440.	2440.

Heat transfer by boiling is characterized by the critical heat flux of the liquid at the design pressure level.

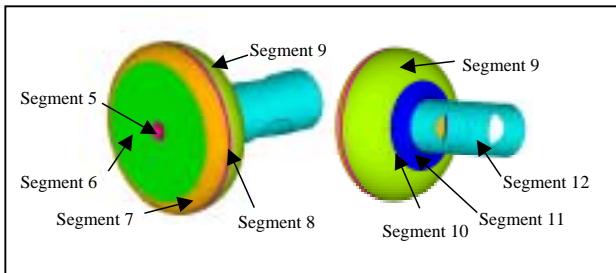


Figure 2, RF Surface segments

Typically under conditions of nucleate boiling heat is transferred from the surface at increasing rates with

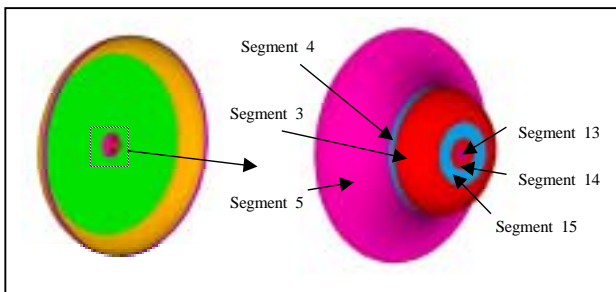


Figure 3, Cathode segments

increasing temperature difference between the surface and saturation temperature of the liquid, figure 4. The critical

heat flux is the point which signifies departure from nucleate boiling, DNB, where the vapor bubbles become large and effectively create an insulating boundary between the fluid and the surface. On the helium bath side of the laser load surfaces, segments 13, 14, and 15, the temperature difference increases (goes to the right of the DNB point, figure 4) and a significant decrease in heat transfer to the boiling liquid is realized. In this three dimensional analysis the heat load spreads through the bulk niobium and into segment 3, which has a much larger surface area, and here the helium bath is adequate to remove the laser load. These effects are included in the model by an appropriate heat transfer coefficient

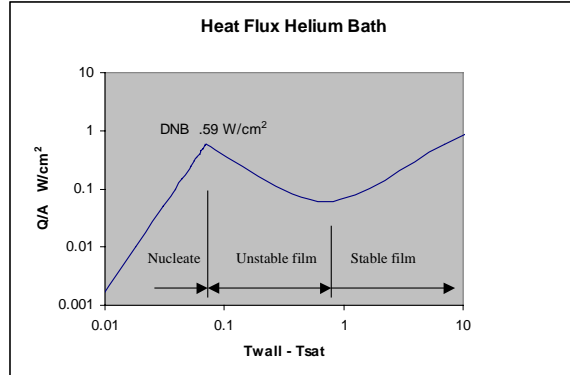


Figure 4, Boiling Helium Heat Flux

developed from  $Q/A/(Tw-Tsat)$ . The curve to the right, figure 4, of the DNB point is assumed by dropping the  $Q/A$  by an order of magnitude for an order of magnitude increase in  $Tw-Tsat$ . The stable film  $Q/A$  points were determined by assuming the DNB  $Q/A$  is recovered after a two order of magnitude increase in  $Tw-Tsat$ . Since the 1 watt average laser power pushes  $Tw-Tsat$  to the right of the DNB, caution must be taken as this power level is approached.

### 3 RESULTS

Results of the thermal analysis are shown in figures 5 and 6. The maximum temperature of 6.9 k is on the cathode surface at the location of the peak heat flux from

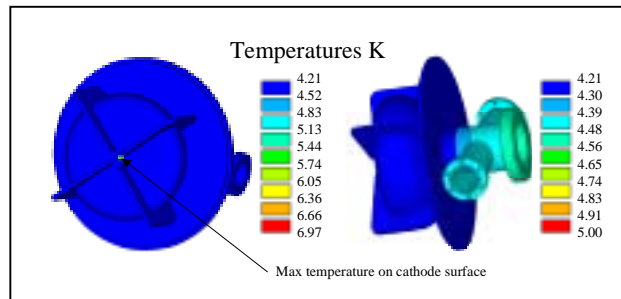


Figure 5, Cavity temperature distribution

the laser. A short distance away from the cathode the niobium temperature decreases to levels which signify that nucleate boiling is the mode of heat transfer, figure 6. The effectiveness of boiling will be dependent on the

local geometry on the helium bath side of the cathode and on the bulk thermal conductivity of the niobium. The analysis was done with a single geometry, no optimization on the wall thickness or the cathode geometry has been completed. Early in the next phase of the program we will evaluate other cathode geometries and optimize the local wall thickness. We will also

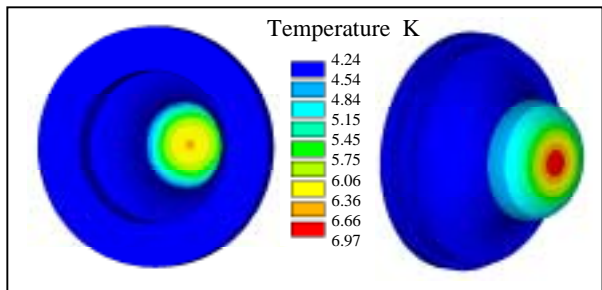


Figure 6, Temperature contours of cathode

consider using superfluid helium, however, preliminary results suggest that due to the high heating rates and significant decrease in thermal conductivity of the niobium from 4K to 2K, no advantage will be realized in the cathode region. However, there will be an overall decrease in the power loss to the cavity walls.

Structural results include pressure differential and the temperature distribution from the 4.2K helium bath. Figures 7 and 8 show the Von Mises stress results. Figure

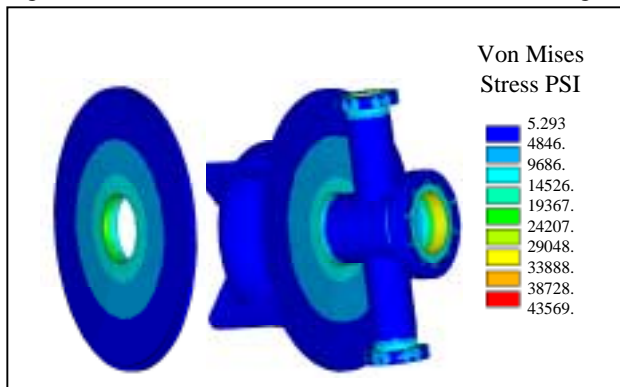


Figure 7, Von Mises Stress in flanges

7 shows stresses that set up at the connection between the stainless steel flanges and the niobium tubes. These stresses are due to the difference in coefficient of thermal expansion between the materials. These connections will be evaluated more thoroughly in the next phase.

Stresses shown on figure 8 are mainly due to the pressure difference between the helium bath and the evacuated cavity. The peak stress is shown on the figure at the edge of the connection between the stiffeners and the cavity. These stresses are low particularly at 4 K where the yield strength for niobium is considerably higher than 5.2 ksi. Stress allowables for niobium RRR250 and welded RRR250 are given in ref [1] as 654 and 466 Mpa respectively.

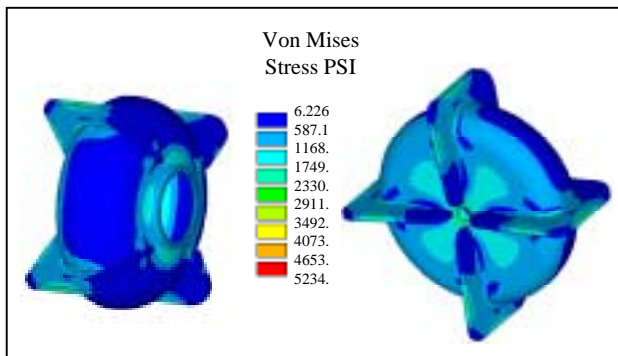


Figure 8, Von Mises contours of cavity

### 4 CONCLUSION

Using the coolant boundary conditions given in figure 4, the temperature of the superconducting niobium cavity will be below the critical temperature of 9.2K at all locations. The assumptions that were made leave some uncertainty and require that the power be brought up to the 1 watt average at a slow rate. Early in the next phase additional studies will be made to optimize the cathode shape and thickness. The geometry of the back of the cathode, which is in contact with the helium bath will also have to be evaluated more closely to avoid inadvertently trapping the boiling vapor.

### REFERENCES

- [1] R. P. Walsh et al, "Low Temperature Tensile and Fracture Toughness Properties of SCRF Cavity Structural Materials"; Proceedings of the Proceedings of the 9th Workshop on RF Superconductivity, Santa Fe, NM 1999.
- [2] H. Padamsee et al., *RF Superconductivity for Accelerators*, John Wiley and Sons, New York, New York, 1998.
- [3] J. Knobloch et al., "High-Field Q Slope in Superconducting Cavities Due to Magnetic Field Enhancement at Grain Boundaries"; Proceedings of the 9th Workshop on RF Superconductivity, Santa Fe, NM, 1999